crystals

MDPI

Article

Centrosymmetric Nickel(II) Complexes Derived from Bis-(Dithiocarbamato)piperazine with 1,1′-Bis(diphenylphosphino)ferrocene and 1,2-Bis(diphenylphosphino)ethane) as Ancillary Ligands: Syntheses, Crystal Structure and Computational Studies

Devyani Srivastava [1], Om Prakash [1], Gabriele Kociok-Köhn [2], Abhinav Kumar [1,*], Abdullah Alarifi [3], Naaser A. Y. Abduh [3], Mohd Afzal [3] and Mohd Muddassir [3,*]

[1] Department of Chemistry, Faculty of Science, University of Lucknow, Lucknow 226 007, India
[2] Materials and Chemical Characterisation Facility (MC2), University of Bath, Claverton Down, Bath BA2 7AY, UK
[3] Department of Chemistry, College of Sciences, King Saud University, Riyadh 11451, Saudi Arabia
* Correspondence: abhinavmarshal@gmail.com (A.K.); muddassir@ksu.edu.sa (M.M.)

Abstract: Two Ni(II) complexes with the formula $[\{Ni(dppf)\}_2\{(L1)_2\}](PF_6)_2$ (Ni-I) and $[\{Ni(dppe)\}_2\{(L1)_2\}](PF_6)_2$ (Ni-II) were prepared by reacting $[Ni(dppf)Cl_2]$ and $[Ni(dppe)Cl_2]$ (dppf = 1,1′-Bis(diphenylphosphino)ferrocene; dppe = 1,2-Bis(diphenylphosphino)ethane) with secondary amine piperazine derived ligand disodium *bis*-(dithiocarbamate)piperazine ($(piper(dtc)_2$ = L1) and counter anion PF_6^-. These complexes were characterized by elemental analyses, FT-IR, ^1H, ^{13}C and ^{31}P NMR, UV-Vis. spectroscopy and single crystal X-ray diffraction. The X-ray analyses reveal centrosymmetric structures where each Ni(II) centre adopts distorted square planar geometry defined by two sulfur centres of dithiocarbamate ligand and two phosphorus centres of dppf and dppe ligands in **Ni-I** and **Ni-II**, respectively. The supramolecular framework of both **Ni-I** and **Ni-II** are sustained by C-H$\cdots\pi$ and C-H$\cdots$F interactions, and they also display interesting intramolecular C-H$\cdots$Ni anagostic interactions. Further, the nature of these interactions are studied using Hirshfeld surface analyses, DFT and quantum theory of atoms in molecules (QTAIM) calculations. Additionally, non-covalent interaction (NCI) plot analyses were conducted to gain additional insight into these non-covalent interactions. This work is vital in a new approach towards the rational designing of the centrosymmetric molecules with interesting architectures.

Keywords: reduced schiff-base; X-ray crystallography; NCI; metal ions

Citation: Srivastava, D.; Prakash, O.; Kociok-Köhn, G.; Kumar, A.; Alarifi, A.; Abduh, N.A.Y.; Afzal, M.; Muddassir, M. Centrosymmetric Nickel(II) Complexes Derived from Bis-(Dithiocarbamato)piperazine with 1,1′-Bis(diphenylphosphino) ferrocene and 1,2-Bis(diphenylphosphino)ethane) as Ancillary Ligands: Syntheses, Crystal Structure and Computational Studies. *Crystals* **2023**, *13*, 343. https://doi.org/10.3390/cryst13020343

Academic Editor: Kil Sik Min

Received: 31 January 2023
Revised: 8 February 2023
Accepted: 15 February 2023
Published: 17 February 2023

1. Introduction

During the past few decades, significant investigations have been conducted on the design and syntheses of coordination complexes comprising varied classes of multifunctional ligands [1–5]. Amongst different varieties of ligands, dithiolates are a crucial class that recently gained attention due to their ability to serve as poly-functional ligands [6,7]. Amongst mono-anionic dithiolates, dithiocarbamates form stable complexes with a wide range of metals in some unusual oxidation states, viz., iron (IV), copper (III), nickel (IV) and gold (III), in symmetric as well as in asymmetric mode and hence exhibited intriguing electrochemical and optical properties [8–12]. In addition, these multifunctional dithiolate ligands can bind to multiple metal centres and can create stable multimetallic aggregates [13–17]. These complexes have industrial applications as lubricating agents, anti-oxidizing agents, fungicides, vulcanizing agents in rubber and emissive materials. Apart from their industrial applications and in view of their interesting crystal engineering aspects and intriguing supramolecular aggregates, investigators working in the area of dithiolates have rationally designed and

synthesized a variety of fascinating novel dithiocarbamate complexes that exhibit intriguing supramolecular structures and photo-physical properties [18]. The supramolecular frameworks in this class of complexes are stabilized by varied non-covalent interactions, such as hydrogen bonding, S···H, O···H, N···H, S···S, C–H···π (chelate, CS_2M), etc. [19,20]. Such non-covalent interactions demonstrate a propensity for supramolecular structures to self-assemble in the solid state through secondary bonds [21]. Such interactions are not only crucial for crystal engineering purpose but facilitate ion transport, sensing and recognition, protein folding, enzyme inhibition and drug interaction with receptors [22–25].

Amongst varied dithiocarbamate-based complexes, nickel (II) complexes offer interesting thermal, electrochemical, catalytic and optical properties. The heteroleptic Ni (II) dithiocarbamate complex has been found to be the potential precursor for nickel sulfides and has displayed potential as electrocatalysts in oxygen evolution reactions (OERs) [26–30]. In addition, they had been used as potential sensitizers in TiO_2-based dye sensitized solar cells (DSSCs) [31–33] and exhibited interesting crystal engineering through varied intermolecular interactions and interesting anagostic Ni···H interactions as well [34,35].

With these aspects in mind and in the quest of newer supramolecular interactions, in this work, two centrosymmetric heteroleptic nickel (II) dithiocarbamates appended with 1,1′-bis(diphenylphosphino) ferrocene (dppf) and 1,2-bis(diphenylphosphino) ethane (dppe) ancillary ligands were synthesized and characterized (Scheme 1). The solid-state structures of both complexes were stabilized by varied interaction, and they also displayed interesting intramolecular C-H···Ni anagostic interactions. The natures of these interactions were addressed with varied computational techniques. The important outcomes of this study are presented herewith.

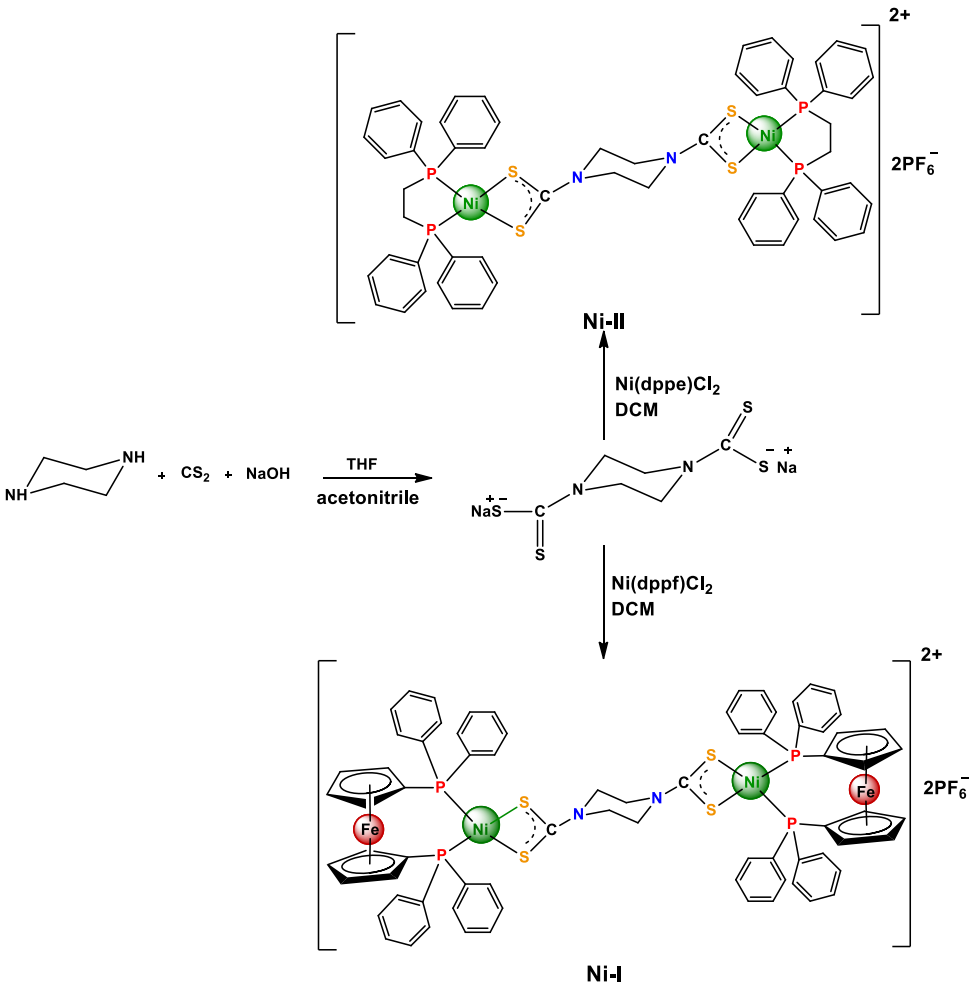

Scheme 1. Synthetic route for preparation of complex **Ni-I** and **Ni-II**.

2. Results and Discussion

2.1. Synthesis

The heteroleptic nickel complex cations with hexafluorophosphate anions were synthesized by reacting disodium piperazine bis-(dithiocarbamate), potassium hexaflorophosphate and Ni(dppf)Cl_2 (**Ni-I**)/Ni(dppe)Cl_2 (**Ni-II**), in methanol and dichloromethane at a suitable stoichiometric ratio [20] (Scheme 1). These complexes were stable under ambient conditions and soluble in halogenated solvents but insoluble in diethyl ether. These compounds were characterized by FTIR, multinuclear NMR spectroscopic techniques and single crystal X-ray diffraction studies.

2.2. Spectroscopy

The FTIR spectroscopic studies for both **Ni-I** and **Ni-II** revealed a band at ~1000 cm^{-1} that could be ascribed to symmetric bidentate vibration of CS_2 of dithiocarbamate moiety. The band appearing at 1435 cm^{-1} arises due to thioureide (N=CS_2) vibration, which indicated the existence of a partial double bond character in N=CS_2 as it is lower that the $\nu_{C=N}$ appearing between 1690–1640 cm^{-1} and ν_{C-N} appearing between the region 1360–1250 cm^{-1} [26–35]. In the ^{1}H NMR spectra of both the complexes, resonances appearing between δ 7.26—7.97 implied the presence of aromatic protons of the dppe and dppf [26–35], while in the case of **Ni-I**, signals corresponding to ferrocene entity appear at δ 4.13–4.30 [26–35]. In ^{13}C NMR, the stout signal at δ 200 ppm corresponds to -CS_2 moiety of bis-dithiocarbamate ligand [26–35], while other upfielded resonances matched well with corresponding aliphatic and aromatic carbons of the main as well as the ancillary ligands. In the $\{^1H\}^{31}P$ NMR spectra, signals at δ −17.9 in **Ni-I** and at δ 62 for **Ni-II** revealed symmetric binding of phosphorus centres of the dppf and dppe ancillary ligands with the Ni(II) core. Additionally, in both complexes, the appearance of a septet at δ 144.3 (J = 712 Hz) corresponded to the hexafluorophosphate counter-anion [26–35]. The electronic absorption spectra for both **Ni-I** and **Ni-II** were recorded dichloromethane solutions (Figure 1a). The strong bands observed between 280–320 nm in the near UV region can be attributed to the intraligand charge transfer transitions, while the appearance of a low energy band in **Ni-I** between 420–580 nm arises due to a *d-d* transition originating from the Fe(II) of ferrocenyl entity along with the contribution from cyclopentadienyl ring orbitals [36–38]. In addition, the appearance of a weak band at ~510 nm arises due to the *d-d* transition corresponding to the Ni(II) centre and suggests square planar geometry around Ni(II) [36]. In addition, the emission spectra for both the complexes were recorded in the solution phase in dichloromethane (Figure 1b). Photoluminescence studies indicated that on excitation at ~310 nm, **Ni-I** displays broad emission at ~368 nm, while **Ni-II** also exhibited broad but relatively less intense emission at 354 nm that could be intraligand charge transfer transitions (Figure 1b) [26–30].

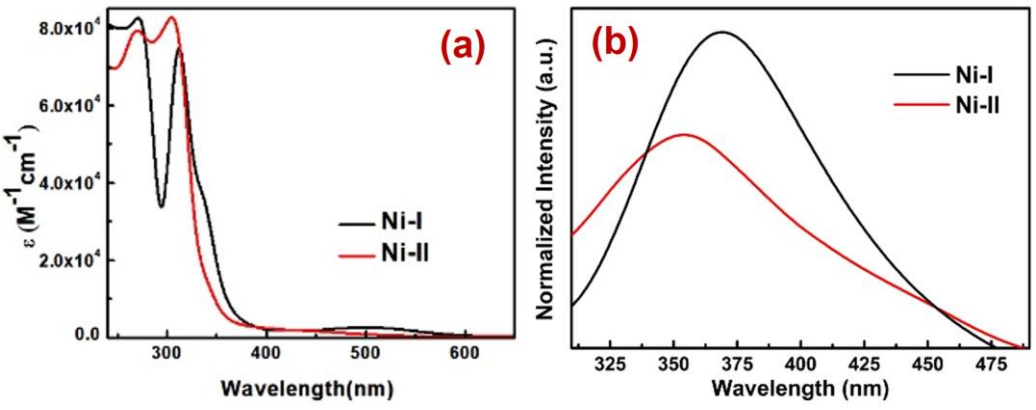

Figure 1. (**a**) Electronic absorption spectra for **Ni-I** and **Ni-II** recorded in 10^{-4} dichloromethane solution; (**b**) emission spectra for **Ni-I** and **Ni-II** recorded in 10^{-4} dichloromethane solution.

2.3. Molecular Structure Description

For **Ni-I**, the single crystals were obtained from the dichlormethane:methanol mixture layered with diethyl ether, while for **Ni-II** the single crystals were grown from the dichlormethane:acetonitrile mixture layered with diethyl ether. The ORTEP view of both complex cations are presented in Figure 2. The structural analyses revealed that **Ni-I** crystallizes in monoclinic crystal system having $P2_1/n$ space group comprising two molecules in the unit cell, while **Ni-II** crystallizes in the triclinic crystal system with P-1 space group having only one molecule in its unit cell. Both complexes are dicationic in nature; hence, to maintain electroneutrality, hexafluorophosphate anions are also present along with the complex cations **Ni-I** and **Ni-II**. The proximal geometry around both the Ni(II) in both complex cations are distorted square planar wherein both Ni(II) centres are coordinated sulfur S1 and S2 of bis-dithiocarbamate ligand. The piperazine ring acquires chair conformation, while the phosphorus centres P1 and P2 dppf and dppe moieties satisfy the rest of the two coordination requirements of both the Ni(II) centres in **Ni-I** and **Ni-II**, respectively. The Ni-S1 and Ni-S2 bond lengths are 2.2220(6) Å and 2.2052(6) Å in **Ni-I,** respectively, while in **Ni-II** they are 2.193(3) Å and 2.207(3) Å. In both complex cations, the bond lengths are nearly identical, thereby suggesting the presence of symmetrical bidentate coordination of the sulfur centres of bis-dithiocarbamate ligands with Ni(II) [34,35]. The Ni-P1 and Ni-P2 bond lengths in **Ni-I** are 2.1970(7) Å and 2.2186(6) Å, respectively, while in **Ni-II** they are 2.149(3) Å and 2.151(3) Å, respectively [34,35]. For **Ni-I**, the bite angles S1-Ni-S2 and P1-Ni-P2 are $78.67(2)^0$ and $99.10(2)^0$, respectively, while in **Ni-II**, the bite angles S1-Ni-S2 and P1-Ni-P2 are $80.57(10)^0$ and $87.21(12)^0$, respectively. The S1-Ni-S2 angle is more acute than the P1-Ni-P2 angle because the dithiocarbamate ligand forms a strained four-membered chelate ring. In both cases, the C-N bond lengths are 1.311(3) Å (**Ni-I**) and 1.300(12) Å (**Ni-II**), respectively, which are intermediate with respect to the C-N (1.47 Å) and C=N (1.28 Å) bonds, indicating a partial double bond character in the thioureide (NCS_2) moiety of bis-(dithiocarbamate) ligand [26]. These bond lengths and geometry around Ni(II) in both complexes are comparable to the previously reported analogous dppe and dppf appended Ni(II)-dithiolates [20,31–35]. In addition, the geometry indices in **Ni-I** and **Ni-II** are 0.16 and 0.05, respectively, which suggest that in both complex cations the geometries are ideally square planar with slight distortions.

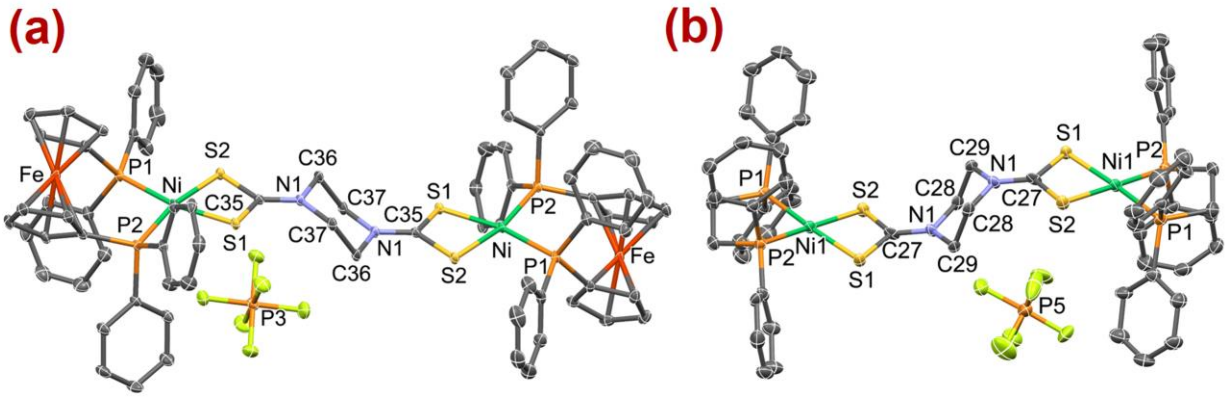

Figure 2. ORTEP view of molecular structures of (**a**) **Ni-I** and (**b**) **Ni-II**. Solvent molecule and hydrogen atoms have been omitted for clarity. Ellipsoids are constructed at 30% probability.

In both **Ni-I** and **Ni-II,** the supramolecular frameworks are sustained by C-H$\cdots\pi$ and C-H$\cdots$F non-covalent interactions (Figures 3 and 4, respectively). In **Ni-I**, two types of C-H$\cdots\pi$ exist. The first one operates between the C7 carbon of the ferrocenyl ring and the H31 hydrogen of the aromatic ring of the dppe ligand. The C-H31$\cdots$C7(π) interaction is 2.787 Å with an angle C-H31$\cdots$C7(π) 165.56° (Figure 3). Another C-H$\cdots\pi$ interaction operates between the C33 carbon of the phenyl ring of the dppf ligand and the H3 hydrogen of the ferrocene ring with C-H2$\cdots$C33(π) distance 2.779 Å and angle 137.80°. Apart from

this, the F4 fluorine of the hexafluorophosphate anion interacts strongly with the H36A hydrogen piperazine unit with H36A· · · F4 distance of 2.481 Å and angle 138.76° (Figure 3).

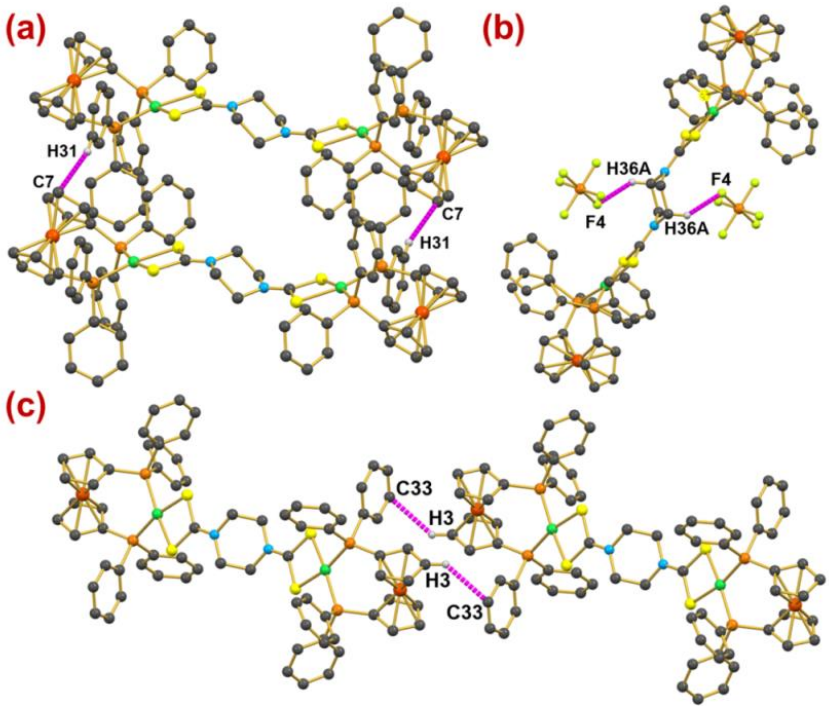

Figure 3. Supramolecular architecture of **Ni-I** indicating the presence of (**a**) and (**c**) C-H· · · π and (**b**) C-H· · · F non covalent interactions.

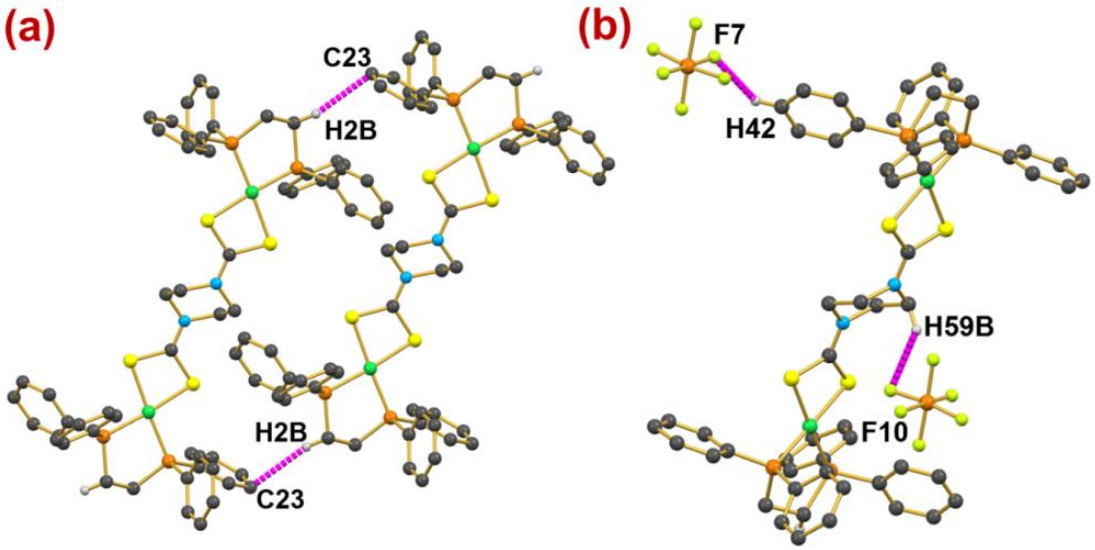

Figure 4. Supramolecular architecture of **Ni-II,** indicating the presence of (**a**) C-H· · · π and (**b**) C-H· · · F non-covalent interactions.

In **Ni-II**, the C-H· · · π interaction exists between the C23 of the phenyl ring carbon of the dppe ligand and the H2B hydrogen of the aliphatic moiety of another dppe ligand (Figure 4). The C-H2B· · · C23(π) interaction distance is 2.786 Å with angle 151.56°. Further, the robustness in the solid state framework of **Ni-II** is further achieved by two C-H· · · F interactions. The first C-H· · · F interaction involves H42 of the aromatic ring of the dppe ligand and F7 of the hexafluorophoshate anion and has separation of 2.540 Å and angle

138.76°, while the second interaction operates between F10 of the hexafluorophoshate anion and H59B of the piperazine unit, having separation of 2.568 Å and angle 140.28°.

Apart from the aforementioned intermolecular interactions, interestingly in both **Ni-I** and **Ni-II** the phenyl hydrogen of the dppf and dppe ligands are lying close to the Ni(II) centre to engender C-H···Ni intramolecular anagostic interactions (Figure 5). The C-H···Ni distances are 2.954 and 2.953 Å long in **Ni-I** and **Ni-II**, respectively, with Ni···H-C angles of 117.0° and 113.9°, respectively, lying in the dimensional value of the anagostic interactions [34]. Unlike agostic interactions, which entail three centre—two electron interactions, these interactions display ionic character (Scheme 2) [34].

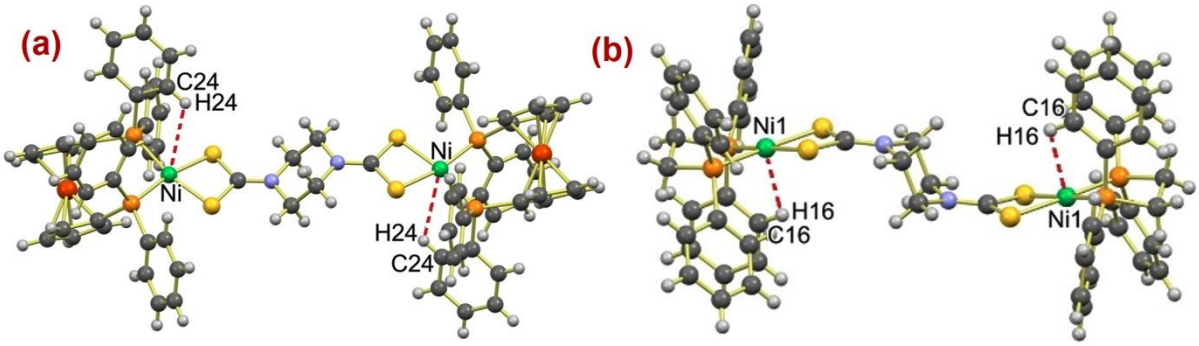

Figure 5. Intramolecular anagostic C-H···Ni interactions for (**a**) **Ni-I** and (**b**) **N-II**.

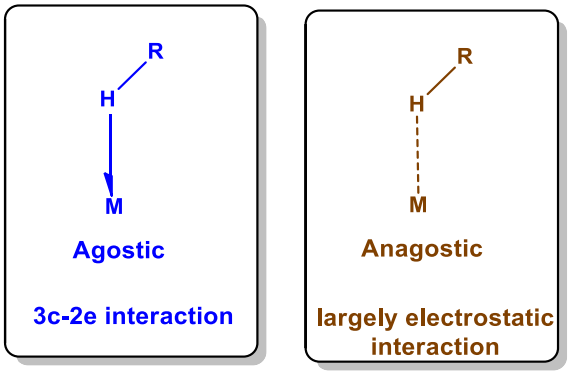

Scheme 2. Scheme depicting basic geometrical differences between agostic and anagostic interactions.

2.4. Hirshfeld Surface Analyses

To assess the nature of weak interactions operating in both complexes, Hirshfeld surface analyses were performed (Figure 6). The Hirshfeld surface of the compounds was mapped over d_{norm} (−0.50 to 1.50 Å), shape index (−1.00 to 1.00 Å) and curvedness (−4.00 to 0.40 Å) [39–42]. In both complexes, strong interactions exist as the red circular depressions on the d_{norm} surface, whereas the prevalence of weak interactions is signified by the light colour depressions (Figure 6). The mode of packing operating in the crystalline state can also be represented by shape index plots, which are sensitive to minor variations in molecular shape caused by irregular deformation generated by nearby crystalline environments. The bumpy patches in both **Ni-I** and **Ni-II** provide evidence for weak interactions that are least impacted by the nearby crystalline environment (Figure 6). Additionally, a closer look at the **Ni-I** surface curvature revealed yellow flecks amid the flat green surfaces, while Ni-II has a flat green surface with red areas that have considerable surface curvature. The red patches in **Ni-II** show that the supramolecular connections involved in creating molecular packing in the single crystal are not iso-energetic in nature in contrast to the yellow patches that highlight the isoenergetic supramolecular contacts in **Ni-I** (Figure 6).

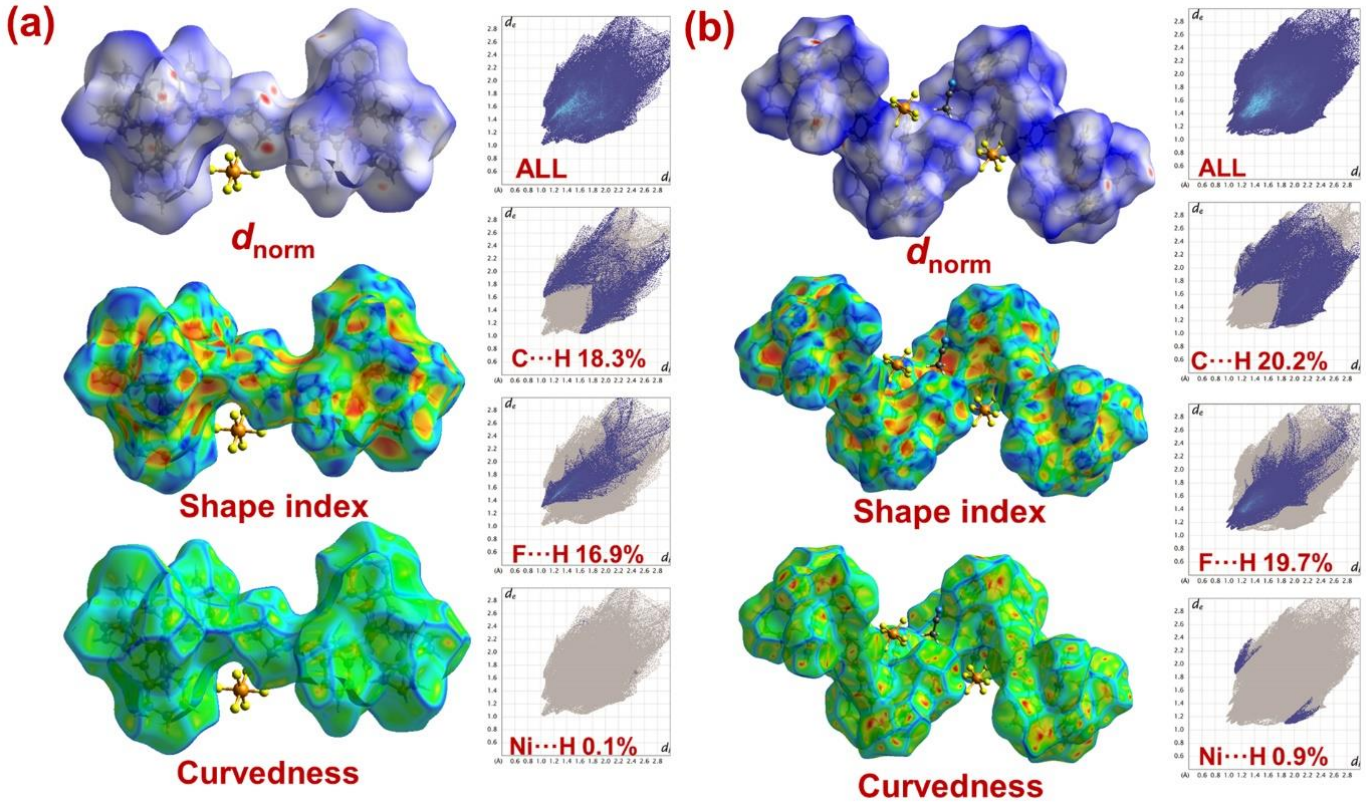

Figure 6. The d_{norm}, shape index, curvedness and fingerprint plots for (**a**) **Ni-I** and (**b**) **Ni-II**.

Apart from the surface analyses, fingerprint plots for both **Ni-I** and **Ni-II** were constructed in which one molecule functions as a donor ($d_e < d_i$), while another behaves like an acceptor ($d_e > d_i$). Additionally, these plots are capable of identifying the atom pairs with close contacts, which provide insight into the better understanding the contributions of the various interactions existing in the crystalline state. In **Ni-I**, the C-H$\cdots\pi$ and C-H$\cdots$F interactions contribute 18.3% and 16.9%, respectively, to the total Hirshfeld surface area, while in **Ni-II** they have percentage contributions of 20.2% and 19.7%, respectively (Figure 6). In both cases, C-H$\cdots\pi$ interaction appeared as a distinct pair of spikes in the 2D region of the fingerprint plots between 1.6 Å $< (d_e + d_i) <$ 2.1 Å. In addition, the C-H$\cdots$F interaction arises as discrete spikes between 1.0 Å $< (d_e + d_i) <$ 2.1 Å in **Ni-I** and 0.9 Å $< (d_e + d_i) <$ 2.1 Å in **Ni-II**. In addition, a meagre C-H···Ni anagostic also exists in the 2D fingerprint plots in both Ni-I and Ni-II with net contributions of 0.1% and 0.9%, respectively.

The propensity of the interatomic contact (X, Y) to create crystal packing interactions has also been evaluated using the enrichment ratio parameter [43–45]. In **Ni-I**, the C-H$\cdots$F interaction with an enrichment ratio of 1.21, had the strongest tendency to produce crystal packing interactions (Table 1), while C-H$\cdots$C and C-H$\cdots$S exhibited enrichment ratios of 1.12 and 1.18, respectively and hence have ability to establish crystal packing interactions (Table 1). In **Ni-II** also the interaction with the highest propensity to form crystal packing interactions for **Ni-II** was C-H$\cdots$F that exhibited an enrichment ratio of 1.38. In addition to C-H$\cdots$F contact, C-H$\cdots$C, C-H$\cdots$N, C$\cdots$C and C-H$\cdots$S contacts also have a stronger potential to create crystal packing interactions, with enrichment ratios of 1.04, 1.17, 1.18 and 1.09, respectively (Table 2).

Table 1. Enrichment ratio of pair of chemical species of **Ni-I**. The enrichment ratio is not calculated for any pair of chemical species for which random contact is less than 0.9%.

Contact %	**Atom**	**H**	**C**	**F**	**N**	**S**	**Ni**
	H	57.7	18.3	16.9	0.3	4.6	0.1
	C	18.3	1.1	0.5	-	-	-
	F	16.9	0.5	-	0.1	0.4	-
	N	0.3	-	0.1	-	-	-
	S	4.6	-	0.4	-	-	-
	Ni	0.1	-	-	-	-	-
Surface%		77.8	10.5	8.95	2.5	0.2	0.45
Random contacts %	Atom	H	C	F	N	S	Ni
	H	60.52					
	C	16.33	1.10				
	F	13.92	1.87	0.80			
	N	0.46	0.04	0.05			
	S	3.89	0.52	0.44	0.01	0.06	
	Ni	0.70	0.09	0.08	0.001	0.02	0.002
Enrichment ratio	Atom	H	C	F	N	S	Ni
	H	0.95					
	C	1.12	1.00				
	F	1.21	0.26				
	N						
	S	1.18					
	Ni						

Table 2. Enrichment ratio of pair of chemical species of Ni-II. The enrichment ratio is not calculated for any pair of chemical species for which random contact is less than 0.9%.

Contact %	**Atom**	**H**	**C**	**F**	**N**	**S**	**Ni**
	H	44.9	20.2	19.7	4.2	5.4	0.9
	C	20.2	2.0	0.5	0.4	1.7	-
	F	19.7	0.5	-	0.4	-	-
	N	4.2	0.4	0.2	-	-	-
	S	5.4	1.7	-	-	-	-
	Ni	0.9	-	-	-	-	-
Surface %		69.75	13.4	10.2	2.45	3.55	0.45
Random contacts %	Atom	H	C	F	N	S	Ni
	H	48.65	-	-	-	-	-
	C	18.69	1.79	-	-	-	-
	F	14.22	2.73	1.04	-	-	-
	N	3.35	0.64	0.49	0.06	-	-
	S	4.95	0.95	0.72	0.17	0.12	0.03
	Ni	0.62	0.1	0.09	0.02	0.03	-
Enrichment ratio	Atom	H	C	F	N	S	Ni
	H	0.92					
	C	1.08	1.11				
	F	1.38	0.18				
	N	1.20					
	S	1.09					
	Ni						

2.5. NCI-RDG

The NCI plot (non-covalent interactions plot) is a technique that is helpful in locating and visualizing non-covalent contacts, including steric hindrance, hydrogen bonds and

Van der Waals interactions [22,46]. In such plots, regions displaying a small decline in density gradient and having low but not zero density serve as indicators of non-covalent interactions. In addition, these interactions are assessed with the help of 3D visualization in the RGB (red–green–blue) color scheme. The blue patches suggest stabilizing interactions, such as hydrogen bonding [47–49], while red regions evince strong repulsive/destabilizing interactions, including ring closure interactions and steric interactions, and the green patches, which are located between the two centres, reveal weak van der Waals interactions. The NCI-RDG plots of **Ni-I** and **Ni-II** presented in Figures 7 and 8, respectively, evince significant non-covalent intermolecular interactions in the form of green patches. Additionally, there are a few small green patches that appear between the monomeric units and are brought on by intramolecular interactions. Apart from this, in both complexes, the red areas appearing at the centre of the aromatic ring evidence the effect of steric repulsion.

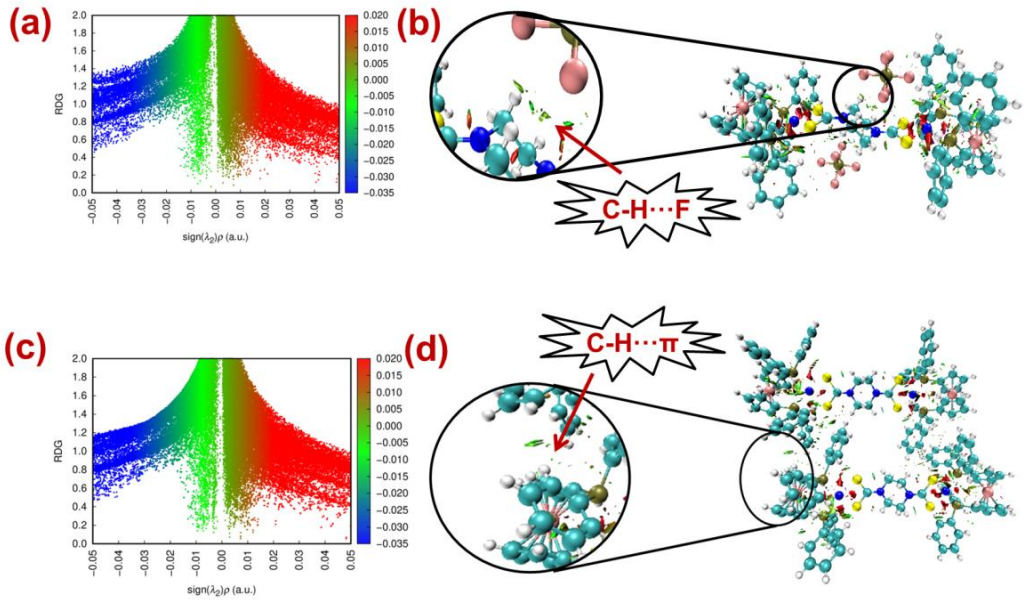

Figure 7. The two-dimensional NCI-RDG plots of reduced density gradient, s, and electron density, ρ, (**a**,**c**) and non-covalent interaction (NCI)-plot visualizing interactions as green surfaces in **Ni-I** (**b**,**d**).

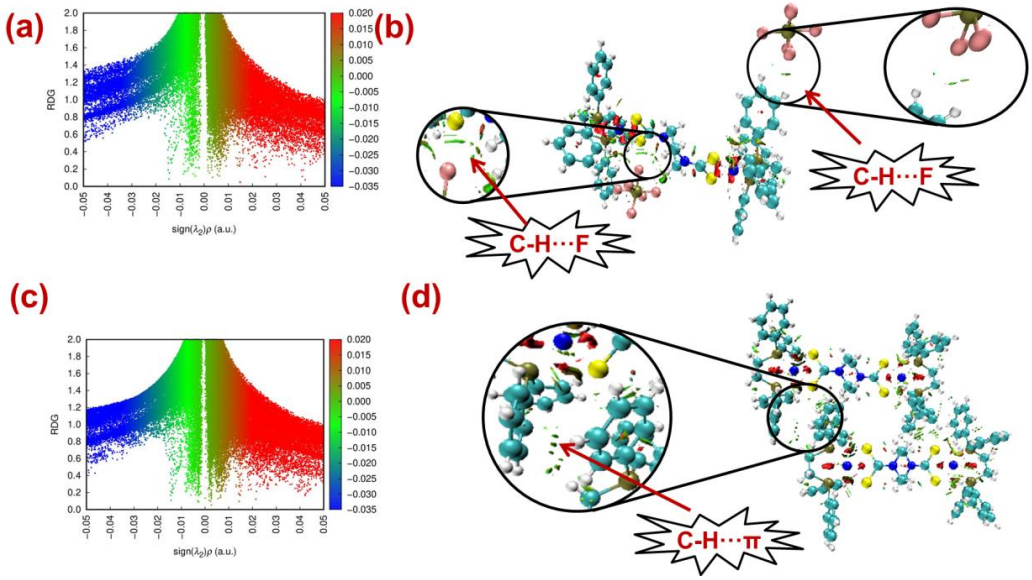

Figure 8. 2D NCI-RDG plots of reduced density gradient, s, and electron density, ρ, (**a**,**c**) and non-covalent interaction (NCI)-plot visualizing interactions as green surfaces in **Ni-II** (**b**,**d**).

2.6. Computational Studies for Non-Covalent Interaction

Using BSSE-corrected B3LYP level theory, non-covalent interaction energies in the crystal structures of both compounds were determined for two neighbouring units held by different non-covalent interactions. The calculated interaction energies for the dimer of the **Ni-I** held by C-H$\cdots\pi$ interactions were 4.0 kJ/mol and 4.1 kJ/mol, while in **Ni-II**, the calculated interaction energy for the dimer held by C-H$\cdots\pi$ interactions was 4.4 kJ/mol. In addition, the calculated interaction energy for C-H$\cdots$F interaction for **Ni-I** was 7.4 kJ/mol, while for **Ni-II**, it was 7.4 kJ/mol.

Further, intermolecular interactions were assessed using QTAIM calculations [47–50]. The existence of bond critical points (bcp) between the interacting atomic centres evinced the existence of non-covalent interactions. In addition, $\boldsymbol{\rho_{bcp}}$ between the interacting atom centres was less than +0.10 au, suggesting the closed-shell nature of these interactions (Table 3) [50–52]. The positive $\boldsymbol{\nabla^2\ \rho_{bcp}}$ values for these interactions provide additional evidence of the decline in electron density between interacting atoms (Table 3) [50–52]. Additionally, the bond ellipticity (ε), which quantifies how well the electron density is constrained along the bond path, suggested the cylindrically asymmetrical nature of these interactions. The weak non-covalent nature of each of these interactions was further demonstrated by the total electron energy density (H), which shows that none of these interactions exhibit substantial sharing of electrons [50–52].

Table 3. Topological parameters for C-S$\cdots\pi$ and C-H$\cdots$F interactions computed for **Ni-I** and **Ni-II**.

Interaction Type	ρ_{bcp}	$\nabla^2\ \rho_{bcp}$	(ε)	H	E (kJ/mol)
		Ni-I			
C31-H31$\cdots$C7	+0.0063	+0.0212	+1.525	0.0011	4.04
C3-H3$\cdots$C33	+0.0043	+0.0319	+1.325	0.0012	4.12
C36-H36A$\cdots$F4	+0.0090	+0.0361	+0.028	0.0023	7.38
		Ni-II			
C2-H2B$\cdots$C23	+0.0060	+0.0190	+0.604	0.0010	3.52
C42-H42$\cdots$F7	+0.0066	+0.0307	+0.148	0.0007	7.18
C59-H59B$\cdots$F10	+0.0052	+0.0265	+0.296	0.0016	4.65

2.7. Wiberg Bond Indices, Mayer Bond Order and Delocalization Index Calculations

The nature of C-H$\cdots$Ni interactions operating within both complex cations were explored using Wiberg bond indices, Mayer bond order and delocalization index calculations. The calculations revealed that in both compounds the Wiberg bond indices for both Ni-I and Ni-II are nearly similar with comparable Mayer atomic bond orders (Table 4). Further, delocalization indices calculation that provide insight regarding the number of electrons shared or exchanged between the two atoms suggested δ(Ni$\cdots$H) (δ = 0.020) are less than ~0.1, suggesting that there is negligible delocalization between the two atomic basins which clearly demonstrates the absence of bond between the two nickel centres. Because anagostic interactions are mostly electrostatic, the natural charges on the coordinated and uncoordinated ortho-hydrogen atoms of the phenyl rings of the dppf and dppe ligands were computed (Table 4). The calculations show that the ortho-hydrogen atoms having anagostic interactions have a lower electron density than ortho-hydrogen atoms located far away from the Ni centre. This supports the occurrence of anagostic interactions in **Ni-I** and **Ni-II**.

Table 4. The C-H···Ni Wiberg bond indices, Mayer bond orders, delocalization indices and natural charges for **Ni-I** and **Ni-II**.

Bond Type	Wiberg Bond Index	Mayer Atomic Bond Order	Delocalization Index (Atom Basin)	Natural Charges	
			Ni-I		
C-H24···Ni	0.0041	0.0073	0.0209	H24	0.2216
				H28 (not displaying C-H···Ni)	0.2134
			Ni-II		
C-H14···Ni	0.0059	0.0112	0.0198	H14	0.2287
				H10 (not displaying C-H···Ni)	0.2102

3. Experimental Procedures

3.1. Materials and Methods

All the reagents and chemicals were commercially available and were used without further purifications. The ligand piperazine-bis(dithiocarbamate) was prepared in accordance with the previously reported method [53]. The FTIR spectral data were collected using Shimadzu IR Affinity-1S spectrometer using KBr disc method. The ^{1}H, ^{13}C and ^{31}P NMR were recorded on a Bruker Avance IIIHD NMR spectrometer using TMS and phosphoric acid as references. Electronic spectral data in dichloromethane solutions were collected on a SPECORD210 spectrophotometer.

3.2. Synthesis

3.2.1. Synthesis of ({Ni(dppf)}$_2$(piperdtc)) (PF_6) (**Ni-I**)

Disodium piperazine bis(dithiocarbamate) (0.070 g, 0.25 mmol) and potassium hexafluorophosphate (0.110 g, 0.6 mmol) were dissolved in methanol and agitated on an ice bath for half an hour. Thereafter, dichloromethane solution of Ni(dppf)Cl_2 (0.342 g, 0.5 mmol) was added to the stirring solution to obtain an orange coloured solution. The reaction mixture was further stirred for another 4 h, and then the solution was rotary evaporated to dryness, dissolved in a minimum amount of dichloromethane and precipitated with diethyl ether. The obtained precipitate was filtered and washed with diethyl ether twice.

Characterization data: Orange–red solid; Yield: 0.350 g, 43.7%.; m.p. 205 °C; ^{1}HNMR (300 MHz, $CDCl_3$, δ): 3.50, 3.97 (m x 2, 8H, NC_4H_8N), 4.24 (s, 4H, Fc), 4.38 (s, 2H, Fc), 4.53 (s, 4H, Fc), 7.26–7.77 (m, C_6H_5, 40H); ^{13}C NMR (75.45 MHz, $CDCl_3$, δ): 205.9(CS_2), 126.9–132.87(-C_6H_5), 29.27(-CH_2-CH_2) ^{31}P NMR (121.54 MHz, $CDCl_3$) −17.9; IR (KBr/cm^{-1}, ν) 1436 (C–N), 1002 (C–S, sym). Elemental Analysis Calc. for $C_{70}H_{64}F_{12}Fe_2Ni_2P_6N_2S_4$ (%): C, 49.33; H, 3.78; N, 1.64; S, 7.53. Found C, 50.12; H, 3.86; N, 1.79; S, 7.98.

3.2.2. Synthesis of ({Ni(dppe)}$_2$(piperdtc))(PF_6)(**Ni-II**)

The **Ni-II** complex using the same procedure except that instead of Ni(dppf)Cl_2 Ni(dppe)Cl_2 (0.264 g, 0.5 mmol) was used.

Characterization data: Orange red solid; Yield: 0.328 g, 45.5%.; m.p. 202 °C; ^{1}HNMR (300 MHz, $CDCl_3$, δ): 2.52 (d, 8H, CH_2-CH_2), 4.14 (s, 8H, C_4H_8), 7.28–7.97 (m, 40H, C_6H_5), ^{13}C NMR (75.45 MHz, $CDCl_3$, δ): 203.8 (CS_2),127.2, 129.8, 132.1, 133.0(C_6H_5) 44.8 (C_4H_8), 26.6 (CH_2– CH_2), ^{31}P NMR (121.54 MHz, $CDCl_3$) 62.35; IR (KBr/cm^{-1}, ν) 1435 (C–N), 1007(C–S, sym). Elemental Analysis Calculated for $C_{58}H_{56}F_{12}Ni_2P_6N_2S_4$ (%): C, 48.36; H, 3.92; N, 1.94; S, 8.90. Found: C, 48.94; H, 4.03; N, 2.12; S, 9.23.

3.3. X-ray Crystallography

The data were collected as per our previous reports employing CrysAlisPro [54], SHELXT [55] and (SHELXL-2018/3) software [55]. Except hydrogens, all atoms were refined anisotropically, while H-atoms were geometrically fixed and refined using a riding model.

3.3.1. Crystallographic Data for Ni-I

$C_{70}H_{64}F_{12}Fe_2Ni_2P_6N_2S_4$, M = 1704.43, Monoclinic, $P2_1/n$, a = 10.51678(13) Å, b = 18.6535(2) Å, c = 20.7494(2) Å, β = 97.4473(11)°, V = 4036.17(8) Å3, Z = 2, D_c = 1.503 mg/m^3, F(000) = 1868, crystal size = 0.480 × 0.151 × 0.102 mm^3, Reflections collected = 42,004, Independent reflections 8016 [R(int) = 0.0552], gof = 1.042, Final R indices [I > 2sigma(I)] R1 = 0.0365, wR2 = 0.0811, R indices (all data) R1 = 0.0457, wR2 = 0.0850, largest diff. peak and hole 0.515 and −0.278 e Å^{-3}. CCDC No. 2236166.

3.3.2. Crystallographic Data for Ni-II

$C_{58}H_{56}F_{12}Ni_2P_6N_2S_4$, M = 1440.55, Triclinic, P-1, a = 9.5191(4) Å, b = 19.3138(8) Å, c = 19.9449(10) Å, α = 73.313(4)°, β = 85.849(4)°, γ = 82.985(4)°, V = 3483.5(3) Å^3, Z = 1, D_c = 1.432 mg/m^3, F(000) = 1538, crystal size = 0.330 × 0.121 × 0.035 mm^3, Reflections collected = 35,018, Independent reflections 12,711 [R(int) = 0.0773], gof = 1.141, Final R indices [I > 2sigma(I)] R1 = 0.1189, wR2 = 0.2396, R indices (all data) R1 = 0.1697, wR2 = 0.2653, largest diff. peak and hole 1.310 and −0.734 e Å^{-3}. CCDC No. 2236167.

3.4. Computational Details

The molecular geometries of dicationic complexes and their dimers were optimized using density functional theory (DFT) by employing the B3LYP functional [56–59]. For all atoms except Ni, a 6-31G** basis set was used, while for Ni, MDF-10 basis sets were employed. The interaction energies were calculated using our previous reports employing the Boys–Bernardi scheme [60]. All computations were performed using the Gaussian 09 revision B.01 programme [61]. QTAIM analyses were performed using AIMALL package version 10.05.04 [62]. The NCI-RDG analysis was performed using the Multiwfn software [63], and the VMD programme was used to create 3D isosurfaces [64]. Additionally, the coloured NCI plots were created using a GNU plot [65].

3.5. Hirshfeld Surface Analyses

Hirshfeld surface analyses were executed by employing the procedure mentioned previously [66–73].

4. Conclusions

In the presented investigation, two piperazine dithiocarbamate based heterometallic complexes of nickel involving 1,2-bis(diphenylphosphino)ferrocene (dppf) and 1,2-bis(diphenylphosphino)ethane (dppe), respectively, were synthesized and characterized. Hirshfeld surface studies, as well as DFT and AIM theory simulations, were used to investigate the nature of weak inter- and intramolecular interactions in these compounds. The fingerprint plots allow for a more complete examination by depicting all of the intermolecular interactions inside the crystal and are thus appropriate for studying changes in crystal packing in the molecular systems under research. In addition, fingerprint plots, Wiberg bond indices, and Mayer bond order calculations were used to verify the anagostic interactions found in the X-ray structures. Based on our findings, we may infer that self-assembled hydrogen bonded and stacking interaction architectures can be altered by carefully designing the nature of the ring and including the right functions on these aromatic rings.

Author Contributions: Conceptualization, A.K.; methodology, O.P. and N.A.Y.A.; software, O.P.; validation, G.K.-K., A.K. and M.A.; formal analysis, D.S., G.K.-K., A.K. and M.A.; investigation, D.S., G.K.-K., A.A., M.A. and M.M.; resources, M.M.; data curation, G.K.-K.; writing—original draft, A.K., M.A. and M.M.; writing—review and editing, D.S., G.K.-K., A.A. and M.M.; visualization, N.A.Y.A.; supervision, M.M.; project administration, M.M.; funding acquisition, M.M. All authors have read and agreed to the published version of the manuscript.

Funding: This research was funded from Deputyship for Research & Innovation, Ministry of Education in Saudi Arabia, for funding this research work through the project number IFKSURG-2-1503.

Acknowledgments: The authors extend their appreciation to the Deputyship for Research & Innovation, Ministry of Education in Saudi Arabia, for funding this research work through the project number IFKSURG-2-1503.

Conflicts of Interest: The author declares no conflict of interest.

References

1. Liu, J.-Q.; Luo, Z.-D.; Pan, Y.; Singh, A.K.; Trivedi, M.; Kumar, A. Recent developments in luminescent coordination polymers: Designing strategies, sensing application and theoretical evidences. *Coord. Chem. Rev.* **2020**, *406*, 213145. [CrossRef]
2. Dutta, A.; Singh, A.; Wang, X.; Kumar, A.; Liu, J. Luminescent sensing of nitroaromatics by crystalline porous materials. *CrystEngComm* **2020**, *22*, 7736–7781. [CrossRef]
3. Silva, P.; Vilela, S.M.F.; Tomé, J.P.C.; Paz, F.A.A. Multifunctional metal–organic frameworks: From academia to industrial applications. *Chem. Soc. Rev.* **2015**, *44*, 6774–6803. [CrossRef] [PubMed]
4. Mendes, R.F.; Figueira, F.; Leite, J.P.; Gales, L.; Paz, F.A.A. Metal–organic frameworks: A future toolbox for biomedicine? *Chem. Soc. Rev.* **2020**, *49*, 9121–9153. [CrossRef]
5. Feng, X.; Liu, J.; Li, J.; Ma, L.-F.; Wang, L.-Y.; Ng, S.-W.; Qin, G.-Z. Series of coordination polymers based on 4-(5-sulfo-quinolin-8-yloxy) phthalate and bipyridinyl coligands: Structure diversity and properties. *J. Sol. State Chem.* **2015**, *230*, 80–89. [CrossRef]
6. Tan, Y.S.; Yeo, C.I.; Tiekink, E.R.T.; Heard, P.J. Dithiocarbamate complexes of platinum group metals: Structural aspects and applications. *Inorganics* **2021**, *9*, 60. [CrossRef]
7. Lee, S.M.; Tiekink, E.R.T. A structural survey of poly-functional dithiocarbamate ligands and the aggregation patterns they sustain. *Inorganics* **2021**, *9*, 7. [CrossRef]
8. Lippard, S.J. Chemistry and molecular biology of platinum anticancer drugs. *Pure Appl. Chem.* **1987**, *59*, 731–742. [CrossRef]
9. Cardell, D.; Hogarth, G.; Faulkner, S. A dithiocarbamate-stabilized copper(I) cube. *Inorg. Chim. Acta.* **2006**, *359*, 1321–1324. [CrossRef]
10. Oyaizu, K.; Yamamoto, K.; Ishii, Y.; Tsuchida, E. Synthesis and characterization of nickel dithiocarbamate complexes bearing ferrocenyl subunits. *Chem. Eur. J.* **1999**, *5*, 3193–3207. [CrossRef]
11. Gimeno, M.C.; Jones, P.G.; Laguna, A.; Sarroca, S.; Calherda, M.J.; Veiros, J. Gold(i) and Gold(iii) Complexes with the 1,1′-Bis (diethyldithiocarbamate) ferrocene Ligand. *Chem. Eur. J.* **1998**, *4*, 2308–2314. [CrossRef]
12. Chant, R.; Hendrickson, A.R.; Martin, R.L.; Rohde, N.M. Metal ion and ligand dependency of the redox behaviour of some first row transition metal dithiocarbamates. *Aust. J. Chem.* **1973**, *26*, 2533–2536. [CrossRef]
13. Beer, P.D.; Berry, N.G.; Cowley, A.R.; Hayes, E.J.; Oates, E.C.; Wong, W.W.H. Metal-directed self-assembly of bimetallic dithiocarbamate transition metal cryptands and their binding capabilities. *Chem. Commun.* **2003**, *19*, 2408–2409. [CrossRef] [PubMed]
14. Wong, W.W.H.; Curiel, D.; Cowley, A.R.; Beer, P.D. Dinuclear zinc(II) dithiocarbamate macrocycles: Ditopic receptors for a variety of guest molecules. *Dalton Trans.* **2005**, *2*, 359–364. [CrossRef] [PubMed]
15. Beer, P.D.; Cheetham, A.G.; Drew, M.G.B.; Fox, O.D.; Hayes, E.J.; Rolls, T.D. Pyrrole-based metallo-macrocycles and cryptands. *Dalton Trans.* **2003**, *4*, 603–611. [CrossRef]
16. Beer, P.D.; Berry, N.; Drew, M.G.B.; Fox, O.D.; Padilla-Tosta, M.E.; Patell, S. Self-assembled dithiocarbamate–copper(II) macrocycles for electrochemical anion recognition. *Chem. Commun.* **2001**, *2*, 199–200. [CrossRef]
17. Padilla-Tosta, M.E.; Fox, O.D.; Drew, M.G.B.; Beer, P.D. Self-assembly of a mixed-valence copper(II)/copper(III) dithiocarbamate catenane. *Angew. Chem. Int. Ed.* **2001**, *40*, 4235–4239. [CrossRef]
18. Fox, O.D.; Drew, M.G.B.; Beer, P.D. Resorcarene-based nanoarchitectures: Metal-directed assembly of a molecular loop and tetrahedron. *Angew. Chem. Int. Ed.* **2000**, *39*, 135–140. [CrossRef]
19. Wilton-Ely, J.D.E.T.; Solanki, D.; Hogarth, G. Multifunctional dithiocarbamates as ligands towards the rational synthesis of polymetallic arrays: An example based on a piperizine-derived dithiocarbamate ligand. *Eur. J. Inorg. Chem.* **2005**, *2005*, 4027–4030. [CrossRef]
20. Knight, E.R.; Leung, N.H.; Lin, Y.H.; Cowley, A.R.; Watkin, D.J.; Thompson, A.L.; Hogarth, G.; Wilton-Ely, J.D.E.T. Multimetallic arrays: Symmetrical bi-, tri-and tetrametallic complexes based on the group 10 metals and the functionalisation of gold nanoparticles with nickel-phosphine surface units. *Dalton Trans.* **2009**, *19*, 3688–3697. [CrossRef]
21. Singh, N.; Kumar, A.; Molloy, K.C.; Mahon, M.F. Syntheses, crystal and molecular structures, and properties of some new phenylmercury(ii) dithiolate complexes. *Dalton Trans.* **2008**, *37*, 4999–5007. [CrossRef] [PubMed]

22. Kumar, P.; Banerjee, S.; Radha, A.; Firdoos, T.; Sahoo, S.C.; Pandey, S.K. Role of non-covalent interactions in the supramolecular architectures of mercury(ii) diphenyldithiophosphates: An experimental and theoretical investigation. *New J. Chem.* **2021**, *45*, 2249–2263. [CrossRef]
23. Arnam, B.V.; Dougherty, D.A. Functional Probes of Drug–Receptor Interactions Implicated by Structural Studies: Cys-Loop Receptors Provide a Fertile Testing Ground: Miniperspective. *J. Med. Chem.* **2014**, *57*, 6289–6300. [CrossRef]
24. Uhlenheuer, D.A.; Petkau, K.; Brunsveld, L. Combining supramolecular chemistry with biology. *Chem. Soc. Rev.* **2010**, *39*, 2817–2826. [CrossRef] [PubMed]
25. Pieters, B.J.G.E.; van Eldijk, M.B.; Nolte, R.J.M.; Mecinović, J. Natural supramolecular protein assemblies. *Chem. Soc. Rev.* **2016**, *45*, 24–39. [CrossRef] [PubMed]
26. Chauhan, R.; Trivedi, M.; Singh, J.; Molloy, K.C.; Kociok-Köhn, G.; Mulik, U.P.; Amalnerkar, D.P.; Kumar, A. 1,2-Bis (diphenylphosphino) ethane nickel(II) dithiocarbamate as potential precursor for nickel sulfide: Effect of counter anion on phase and morphology. *Inorg. Chim. Acta* **2014**, *415*, 69–74. [CrossRef]
27. Singh, A.; Singh, A.; Kociok-Köhn, G.; Molloy, K.C.; Singh, A.K.; Kumar, A.; Muddassir, M. Ni(ii) dithiolate anion composites with two-dimensional materials for electrochemical oxygen evolution reactions (OERs). *New J. Chem.* **2021**, *45*, 16264–16270. [CrossRef]
28. Yadav, R.; Singh, A.; Waghadkar, Y.; Kociok-Köhn, G.; Kumar, A.; Chauhan, R.; Rane, S.; Gosavi, S. 1,2-Bis (diphenylphosphino) ethane nickel(II) O, O′-dialkyldithiophosphates as potential precursors for nickel sulfides. *New J. Chem.* **2017**, *41*, 1327–1333. [CrossRef]
29. Singh, A.; Yadav, R.; Kociok-Köhn, G.; Trivedi, M.; Azad, U.P.; Singh, A.K.; Kumar, A. Syntheses of nickel sulfides from 1,2-bis(diphenylphosphino) ethane nickel(II) dithiolates and their application in the oxygen evolution reaction. *Int. J. Hydrogen Energy* **2018**, *43*, 5985–5995. [CrossRef]
30. Yang, L.; Powell, D.R.; Houser, R.P. Structural variation in copper(I) complexes with pyridylmethylamide ligands: Structural analysis with a new four-coordinate geometry index, τ 4. *Dalton Trans.* **2007**, 955–964. [CrossRef]
31. Singh, A.; Dutta, A.; Singh, A.K.; Trivedi, M.; Kociok-Köhn, G.; Muddasir, M.; Kumar, A. Tertiary phosphine-appended transition metal ferrocenyl dithiocarbamates: Syntheses, Hirshfeld surface, and electrochemical analyses. *Appl. Organomet. Chem.* **2020**, *34*, e5879. [CrossRef]
32. Singh, A.; Singh, P.; Kociok-Köhn, G.; Trivedi, M.; Kumar, A.; Chauhan, R.; Rane, S.B.; Terashima, C.; Gosavi, S.W.; Fujishma, A. 1,1′-Bis(diphenylphosphino) ferrocene-appended nickel(II) dithiolates as sensitizers in dye-sensitized solar cells. *New J. Chem.* **2018**, *42*, 9306–9316. [CrossRef]
33. Singh, A.; Dutta, A.; Srivastava, D.; Kociok-Köhn, G.; Chauhan, R.; Gosavi, S.; Kumar, A.; Muddassir, M. Effect of different aromatic groups on photovoltaic performance of 1,1′-bis(diphenylphosphino) ferrocene functionalized Ni(II) dithiolates as sensitizers in dye sensitized solar cells. *Appl. Organomet. Chem.* **2021**, *35*, e64022021. [CrossRef]
34. Yadav, R.; Trivedi, M.; Kociok-Köhn, G.; Prasad, R.; Kumar, A. New Ni(II) 1,2-bis(diphenylphosphino) ethane dithiolates: Crystallographic, computational and Hirshfeld surface analyses. *CrystEngComm* **2015**, *17*, 9175–9184. [CrossRef]
35. Singh, A.; Singh, A.; Kociok-Köhn, G.; Chauhan, R.; Gosavi, S.W.; Singh, A.; Singh, A.K.; Kumar, A.; Muddassir, M. Phase-controlled solvothermal syntheses and oxygen evolution reaction (OER) activity of nickel sulfide nanoparticles obtained from 1,2-bis(diphenylphosphino) ethane nickel(ii) acetylacetonatedithiolate. *New J. Chem.* **2022**, *46*, 10246–10255. [CrossRef]
36. Singh, V.; Chauhan, R.; Kumar, A.; Bahadur, L.; Singh, N. Efficient phenylmercury(II) methylferrocenyldithiocarbamate functionalized dye-sensitized solar cells. *Dalton Trans.* **2010**, *39*, 9779–9788. [CrossRef]
37. Barnsley, J.E.; Findlay, J.A.; Shillito, G.E.; Pellet, W.S.; Scottwell, S.; Mcintyre, S.M.; Tay, E.T.; Gordon, K.C.; Crowley, J.D. Long-lived MLCT states for Ru(II) complexes of ferrocene-appended 2,2′-bipyridines. *Dalton Trans.* **2019**, *48*, 15713–15722. [CrossRef]
38. Lever, A.B.P. *Inorganic Electronic Spectroscopy*; Elsevier: Amsterdam, The Netherlands, 1984; pp. 479–507.
39. Singh, A.; Singh, A.; Srivastava, D.; Kociok-Köhn, G.; Köhn, R.D.; Kumar, A.; Muddassir, M. New di-n-butyltin(iv)-bis-(1-alkoxy-isoquinoline-4-nitrile thiolate): Crystallographic and computational studies. *CrystEngComm* **2022**, *24*, 4274–4282. [CrossRef]
40. Singh, P.; Singh, A.; Singh, A.; Singh, A.K.; Kociok-Köhn, G.; Alowais, A.; Abduh, N.A.Y.; Muddassir, M.; Kumar, A. New 1D diorganotin(IV) dithiolate coordination polymers: Crystallographic, computational, Hirshfeld surface and thermal analyses. *CrystEngComm* **2020**, *22*, 2049–2059. [CrossRef]
41. Kumar, A.; Singh, A.; Yadav, R.; Singh, S.; Kociok-Köhn, G.; Trivedi, M. Supramolecular architecture of organotin(IV) N-methyl ferrocenyl N-ethanol dithiocarbamates: Crystallographic and computational studies. *Inorg. Chim. Acta* **2018**, *471*, 234–243. [CrossRef]
42. Yadav, R.; Trivedi, M.; Chauhan, R.; Prasad, R.; Kociok- Köhn, G.; Kumar, A. Supramolecular architecture of organotin(IV) 4-hydroxypiperidine dithiocarbamates: Crystallographic, computational and Hirshfeld surface analyses. *Inorg. Chim. Acta* **2016**, *450*, 57–68. [CrossRef]
43. Jelsh, C.; Ejsmont, K.; Huder, L. The enrichment ratio of atomic contacts in crystals, an indicator derived from the Hirshfeld surface analysis. *IUCrJ* **2014**, *1*, 119–128. [CrossRef] [PubMed]
44. Ali, A.; Ashfaq, M.; Din, Z.U.; Ibrahim, M.; Khalid, M.; Assiri, M.A.; Riaz, A.; Tahir, M.N.; Rodrigues-Filho, E.; Imran, M.; et al. Synthesis, Structural, and Intriguing Electronic Properties of Symmetrical Bis-Aryl-α, β-Unsaturated Ketone Derivatives. *ACS Omega* **2022**, *7*, 39294–39309. [CrossRef]

45. Askerov, R.K.; Ashfaq, M.; Chipinsky, E.V.; Osmanov, V.K.; Tahir, M.N.; Baranov, E.V.; Fukin, G.K.; Khrustalev, V.N.; Nazarov, R.H.; Borisova, G.N.; et al. Synthesis, crystal structure, exploration of the supramolecular assembly through Hirshfeld surface analysis and bactericidal activity of the cadmium organometallic complexes obtained from the heterocyclic ligand. *Results Chem.* **2022**, *4*, 100600. [CrossRef]
46. Chiter, C.; Bouchama, A.; Nardjes Mouas, T.; Allal, H.; Yahiaoui, M.; Warad Il Zarrouk, A.; Djedouani, A. Synthesis, crystal structure, spectroscopic and hirshfeld surface analysis, NCI-RDG, DFT computations and antibacterial activity of new asymmetrical azines. *J. Mol. Struc.* **2020**, *1217*, 128376. [CrossRef]
47. Foroutan-Nejad, C.; Shahbazian, S.; Marek, R. Toward a consistent interpretation of the QTAIM: Tortuous link between chemical bonds, interactions, and bond/line paths. *Chem. Eur. J.* **2014**, *20*, 10140. [CrossRef]
48. Sowlati-Hashjin, S.; Šadek, V.; Sadjadi, S.; Karttunen, M.; Martín-Pendás, A.; Foroutan-Nejad, C. Collective interactions among organometallics are exotic bonds hidden on lab shelves. *Nat. Commun.* **2022**, *13*, 2069. [CrossRef]
49. Matito, E.; Poater, J.; Solà, M.; Duran, M.; Salvador, P. Comparison of the AIM delocalization index and the mayer and fuzzy atom bond orders. *J. Phys. Chem. A* **2005**, *43*, 9904–9910. [CrossRef]
50. Bader, R.F.W. *Atoms in Molecules: A Quantum Theory*; Oxford University Press: New York, NY, USA, 1990.
51. Matta, C.F.; Boyd, R.J. *The Quantum Theory of Atoms in Molecules: From Solid State to DNA and Drug Design*; Wiley VCH, Verlag Gmbh & Co.: KGaA, Germany, 2007.
52. Matta, C.F.; Hernandez-Tryjillo, J.; Tang, T.H.; Bader, R.F.W. Hydrogen–hydrogen bonding: A stabilizing interaction in molecules and crystals. *Chem. Eur. J.* **2003**, *9*, 1940. [CrossRef]
53. Kumar, A.; Mayer-Figge, H.; Sheldrick, W.S.; Singh, N. Synthesis, structure, conductivity, and calculated nonlinear optical properties of two novel bis(triphenylphosphane)copper(I) dithiocarbamates. *Eur. J. Inorg. Chem.* **2009**, *2009*, 2720–2725. [CrossRef]
54. *Rigaku Oxford Diffraction*, version 1.171.40.67a; CrysAlisPro; Rigaku Oxford Diffraction: Tokyo, Japan, 2019.
55. Sheldrick, G.M. Crystal structure refinement with SHELXL. *Acta Cryst.* **2015**, *71*, 3–8.
56. Becke, A.D. Density-functional thermochemistry. III. The role of exact exchange. *J. Chem. Phys.* **1993**, *98*, 5648–5652. [CrossRef]
57. Lee, C.; Yang, W.; Parr, R.G. Development of the Colle-Salvetti correlation-energy formula into a functional of the electron density. *Phys. Rev. B* **1988**, *37*, 785–789. [CrossRef] [PubMed]
58. Vosko, S.H.; Wilk, L.; Nusair, M. Accurate spin-dependent electron liquid correlation energies for local spin density calculations: A critical analysis. *Can. J. Phys.* **1980**, *58*, 1200–1211. [CrossRef]
59. Stephens, P.J.; Devlin, F.J.; Chabalowski, C.F.; Frisch, M.J. Ab initio calculation of vibrational absorption and circular dichroism spectra using density functional force fields. *J. Phys. Chem.* **1994**, *98*, 11623–11627. [CrossRef]
60. Boys, S.F.; Bernardi, F. The calculation of small molecular interactions by the differences of separate total energies. Some procedures with reduced errors. *Mol. Phys.* **1970**, *19*, 553. [CrossRef]
61. Frisch, M.J.; Trucks, G.W.; Schlegel, H.B.; Scuseria, G.E.; Robb, M.A.; Cheeseman, J.R.; Montgomery, J.A.; Vreven, T., Jr.; Kudin, K.N.; Burant, J.C.; et al. *Gaussian 09 Revision B.01*; Gaussian, Inc.: Wallingford, CT, USA, 2009.
62. Keith, T.A.; Gristmill, T.K. *Software*; TK Gristmill Software: Overland Park, KS, USA; Available online: Aim.tkgristmill.com (accessed on 31 January 2023).
63. Lu, T.; Chen, F. Multiwfn: A multifunctional wavefunction analyzer. *J. Comput. Chem.* **2012**, *33*, 580–592. [CrossRef]
64. Humphrey, W.; Dalke, A.; Schulten, K.J. VMD: Visual molecular dynamics. *J. Mol. Graph.* **1996**, *14*, 33–38. [CrossRef]
65. Williams, T.; Kelley, C. 1986–1993, 1998, 2004, 2007–2022. Available online: www.gnuplot.info (accessed on 31 January 2023).
66. Spackman, M.A.; McKinnon, J.J. Fingerprinting intermolecular interactions in molecular crystals. *CrystEngComm* **2002**, *4*, 378. [CrossRef]
67. Spackman, M.A.; Byrom, P.G. A novel definition of a molecule in a crystal. *Chem. Phys. Lett.* **1997**, *267*, 309. [CrossRef]
68. McKinnon, J.J.; Mitchell, A.S.; Spackman, M.A. Hirshfeld surfaces: A new tool for visualising and exploring molecular crystals. *Chem-Eur. J.* **1998**, *4*, 2136. [CrossRef]
69. McKinnon, J.J.; Spackman, M.A.; Mitchell, A.S. Novel tools for visualizing and exploring intermolecular interactions in molecular crystals. *Acta Crystallogr. Sec. B* **2004**, *60*, 627. [CrossRef]
70. Rohl, A.L.; Moret, M.; Kaminsky, W.; Claborn, K.; McKinnon, J.J.; Kahr, B. Hirshfeld surfaces identify inadequacies in computations of intermolecular interactions in crystals: Pentamorphic 1,8-dihydroxyanthraquinone. *Cryst. Growth Des.* **2008**, *8*, 4517. [CrossRef]
71. Parkin, A.; Barr, G.; Dong, W.; Gilmore, C.J.; Jayatilaka, D.; McKinnon, J.J.; Spackman, M.A.; Wilson, C.C. Comparing entire crystal structures: Structural genetic fingerprinting. *CrystEngComm* **2007**, *9*, 648. [CrossRef]
72. Wolff, S.K.; Greenwood, D.J.; McKinnon, J.J.; Jayatilaka, D.; Spackman, M.A. *Crystal Explorer 3.1*; University of Western Australia: Perth, Australia, 2012.
73. Koenderink, J.J.; Van Doorn, A.J. Surface shape and curvature scales. *Image Vision Comput.* **1992**, *10*, 557. [CrossRef]